European Journal of Environmental and Civil Engineering

ISSN: 1964-8189 (Print) 2116-7214 (Online) Journal homepage: https://www.tandfonline.com/loi/tece20

Viscoelastic-plastic constitutive model with non-constant parameters for brittle rock under high stress conditions

Shuling Huang, Chuanqing Zhang, Xiuli Ding & Liu Yang

To cite this article: Shuling Huang, Chuanqing Zhang, Xiuli Ding & Liu Yang (2020): Viscoelastic-plastic constitutive model with non-constant parameters for brittle rock under high stress conditions, European Journal of Environmental and Civil Engineering, DOI: 10.1080/19648189.2020.1740893

To link to this article: https://doi.org/10.1080/19648189.2020.1740893

EUROPEAN JOURNAL OF ENVIRONMENTAL AND CIVIL ENGINEERING
https://doi.org/10.1080/19648189.2020.1740893

Viscoelastic-plastic constitutive model with non-constant parameters for brittle rock under high stress conditions

Shuling Huang[a], Chuanqing Zhang[b,c], Xiuli Ding[a] and Liu Yang[b,c]

[a]Key Laboratory of Geotechnical Mechanics and Engineering of Ministry of Water Resources, Yangtze River Scientific Research Institute, Wuhan, Hubei, China; [b]State Key Laboratory of Geomechanics and Geotechnical Engineering, Institute of Rock and Soil Mechanics, Chinese Academy of Sciences, Wuhan, Hubei, China; [c]University of Chinese Academy of Sciences, Beijing, China

ABSTRACT

Under the long-term effect of high stress, the stability problem caused by the time-dependent deformation of brittle surrounding rock in deep engineering is becoming more and more prominent. The accurate description of the effectiveness of brittle rock is an important basis for the prediction of mechanical response and the stability evaluation of surrounding rock in deep engineering. To describe the accelerated time-dependent deformation behavior of brittle rock, a Newtonian body with non-constant parameters considering the effects of stress state is proposed. Combined with the improved Burgers model, a viscoelastic model with non-constant parameters of brittle rock is developed. The effects of time, delay coefficient, and stress level on the viscosity coefficient, as well as the influence of delay coefficient and initial viscosity coefficient on the accelerated time-dependent deformation, are examined. The results show that (1) the viscosity coefficient decreases with time and increases with the delay coefficient, while the attenuation rate increases; (2) the viscosity coefficient decreases with increasing stress level, and its attenuation rate increases with time; (3) with the increase of the delay coefficient, the nonlinear characteristics of the accelerated phase of the rock time-dependent deformation curve become more and more obvious; and (4) as the initial viscosity coefficient increases, the nonlinear characteristics of the accelerated phase of the time-dependent deformation curve become less and less obvious. The above laws fully reflect the evolutionary law of the nonlinear time-dependent deformation of rock. By comparing the results of the marble creep test with theoretical predictions, we found that when the stress limit is exceeded, the established model can well describe the initial attenuation, steady state, and accelerated characteristics of the rock time-dependent deformation curve, thus verifying the ability of the proposed model to describe the accelerated creep behavior, as well as the overall rationality of the model.

ARTICLE HISTORY
Received 7 October 2019
Accepted 6 March 2020

KEYWORDS
Viscoelastic-plastic; non-constant parameters; Burgers; viscosity coefficient; brittle rock; accelerated creep

1. Introduction

Following the excavation and support of a deep underground engineering project, the surrounding rock suffers from hysteresis along with continuous deformation and destruction. These phenomena reflect the time-dependent mechanical behavior and properties of rock under high stress. Existing research results

CONTACT Chuanqing Zhang cqzhang@whrsm.ac.cn State Key Laboratory of Geomechanics and Geotechnical Engineering, Institute of Rock and Soil Mechanics, Chinese Academy of Sciences, Wuhan, Hubei 430071, China

have primarily focused on the large deformation of weak rock rheology, while Martin and Chandler (1994), Read et al. (1998), and Szczepanik et al. (2003) found that hard rock under high stress also has significant time-dependent properties. As the scale of construction projects continues to increase and the environmental conditions tend to become more severe, the engineering problems caused by the time-dependent properties of the brittle rock become more and more prominent. In the Jinping II Hydropower Station of China project, after 150 days of excavating the diversion tunnel, the damage zone depth of the rock surrounding the excavation increased by 1.3 m (Feng et al., 2016). The Jinping auxiliary tunnel is supported by the system of spray anchoring. After nearly 10 years of operation, time-dependent damage of the surrounding rock is still occurring. Therefore, as a large number of deep underground engineering projects are completed and begin operation, the long-term safety state evolution, evaluation, and prediction of engineering under high geostress conditions are key issues in the attempt to ensure operational safety, and there is an urgent need to accurately describe the time-dependent mechanical behavior of hard and brittle rock under high stress conditions.

In the field of rock mechanics, there are many constitutive models specifically used to describe the rheological behavior of soft rock, but in general they can be grouped into two categories: either the empirical rheological constitutive model or the component combination rheological model. The rock empirical rheological constitutive model can only reflect the rheological mechanical properties of rock under specific stress paths or stress states, and does not have universal applicability for different rock types or engineering projects. The component combination rheological model is obtained by series and parallel connection of elastic, plastic, and viscous mechanical elements (i.e., the Hooke body, Saint Venant body, and Newtonian body) in different forms, and corresponding creep and relaxation equations can be obtained under specific stress and strain conditions. Since the component combination rheological model has a simple concept and a clear physical meaning, it can comprehensively reflect various rheological properties such as creep, relaxation, and elastic after-effect. Therefore, this type of model has been widely used. Representative component combination rheological models include the Maxwell model, Kelvin model, Kelvin-Voigt model, Burgers model, Bingham model, and Nishihara model.

However, since traditional component combination models are composed of linear components, they cannot describe the accelerated creep phase of the rock. To this end, scientists have conducted extensive and in-depth research on the theory of nonlinear rock rheology, and have achieved many meaningful results. Chan et al. (1992, 1994, 1996) and Fossum et al. (1993) introduced continuous damage mechanics into the rheological analysis of rock salt, pointing out that the creep caused by rock salt damage accumulates from the transitional creep stage to the accelerated creep phase, and then proposing a rock salt creep damage fracture coupling model. Boukharov et al. (1995) proposed a viscous damping element with a certain mass and a finite damping column length to simulate the tertiary creep of rock, and it was proved that this model can be used to describe the nonlinear creep of brittle crystalline rock. Dashnor et al. (2005) used a meso-damage mechanics theory to establish a three-stage creep rheological model that describes the long-term properties of natural gypsum rock. Fabre and Pellet (2006) believe that there is a certain stress threshold switch between steady-state creep and accelerated creep. When the load stress is less than the stress threshold, the rock only exhibits the initial creep phase, and when the load stress is greater than the stress threshold, the steady state and accelerated creep phases occur. Sterpi and Gioda (2009) established a rock creep model considering viscoelasticity and viscoplasticity, which also took into account the effects of accelerated creep, including progressive mechanical damage dominated by cumulative viscoplastic strain. Nedjar and Roy (2013) used a continuous damage mechanics method to include a damage factor in the creep model to describe the accelerated creep phase. Barla et al. (2012) and Fahimifar et al. (2015), respectively proposed nonlinear rheological models and viscoplastic models to describe the accelerated creep phase. It can be seen that the current rheological constitutive models that can describe the tertiary stage or the accelerated creep phase are mostly for soft rock; the related models specifically for hard and brittle rock are rare.

During the creep deformation process of rock under high stress, the internal cracking of the rock initiates, expands, and causes damage, and with the accumulation of damage, the rheological mechanical properties of the rock also change, and the mechanical parameters in the rheological constitutive model change from constant to non-constant (Zhang et al., 2016, 2018). Therefore, if the rock rheological mechanical parameters are regarded as non-constant parameters and used to characterize the damage degradation process of the rock, the time-dependent characteristics of the rock mass will be more directly and objectively reflected. Gioda (1981) first studied the nonlinear properties of rock materials and concluded

that the viscosity coefficient η should be a function of time and independent of stress levels. Subsequently, Vyalov (1986) proposed a modified Bingham's law considering the non-linear relationship between flow rate and stress based on the assumption that the isochronal stress–strain curves are similar, and changed the viscosity coefficient of the "viscous pot" in the Bingham model into a nonlinear parameter, thereby deducing the corresponding nonlinear creep constitutive model. Cristescu (1987, 1993) believed that viscosity coefficient is not constant but dependent possibly on stress, strain and damage history. And the viscosity coefficient of salt rock is generally mainly related to stress, other variables such as, for instance, strain, damage, humidity and temperature may also be involved, if necessary.

In recent years, viscosity coefficient is considered to be a function of the accumulation of damage. Liu et al. (2016) and Tang et al. (2018) respectively studied the accelerated creep phase of soft coal and salt rock and concluded that the relationship between viscosity coefficient and time complies with the law of exponential attenuate, and the attenuation index is the damage time factor. Zhao et al. (2018) proposed that the viscous coefficient can be expressed as an exponential function based on the creep test results of shale, the exponent of the function are related to the stress levels and cycle times. Wang et al. (2017) assumed that the viscous coefficient can be a 2-parameter Weibull cumulative distribution function based on the triaxial compression creep test of granite according to fractal theory. Zhang et al. (2019) used an exponential function to fit the accelerated creep phase of the multistage creep test of coal, and proposed that the viscous coefficient is a time-dependent exponential function.

The most important characteristics of the time-dependent mechanical behavior of hard brittle rock are closely related to the stress conditions. Under low stress, this behavior is characterized by attenuating time-dependent deformation. As the stress rises, it changes to steady-state time-dependent deformation. When the stress reaches the damaging level, it quickly enters the phase of accelerated time-dependent deformation. Due to the brittle nature of the rock itself, its viscosity coefficient varies with stress level and time, its accelerated rheological phase is generally much shorter than that of the soft rock that has been studied, and its deformation rate is large. Current viscoelastic plastic models for soft rock have difficulty describing these time-dependent mechanical properties of hard brittle rock well.

To address this issue, based on component theory, this study proposes utilizing the Newtonian body with non-constant parameters (called the non-constant Newtonian body below) taking into account the effect of the stress state to describe the accelerated time-dependent deformation behavior of hard brittle rock. Based on the effects of the delay coefficient and time on the viscosity coefficient, as well as the effects of the delay coefficient and initial viscosity coefficient on the accelerated time-dependent deformation, in combination with the improved Burgers model, the viscoelastic model with non-constant parameters (called the non-constant viscoelastic model below) of hard brittle rock is established. This model describes the three-phase time-dependent deformation law of initial deformation as well as the steady state and accelerated phase. The corresponding creep and relaxation equations are derived and the rationality of the established model is verified by comparing the theoretical results with the experimental results.

2. Viscoplastic model with non-constant parameters based on a Bingham body

Instantaneous failures and creep failures of hard-brittle rock are induced by initiation, propagation, aggregation, and connection of internal cracks. When the stress exceeds the long-term strength, the bearing capacity of rock under the same deformation rate declines over time, i.e., with the propagation of internal cracks, the viscosity gradually decreases and the rock is damaged when the strain reaches the critical value. Additionally, the aforementioned process is also influenced by stress level, i.e., different stress levels result in differing amounts of time until rock failure: the higher the stress, the lower the viscosity, and the earlier the failure. When the stress exceeds a certain value, the isochronous stress–strain curve exhibits non-linearity, showing deformation at an accelerated rate. Although the generally applied Bingham model can describe the viscoplastic characteristics of rock, it fails to describe the accelerated creep phase. Therefore, based on the Bingham model, a non-constant Newtonian body taking into account the influence of stress state is proposed, as shown in Figure 1.

According to the characteristics of the strain-time curve during the accelerated creep phase of the test, the function relationship between strain and time is as follows:

$$\varepsilon(t) = (At + Bt^3)(\sigma - \sigma_s), \tag{1}$$

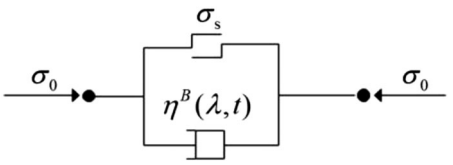

Figure 1. Bingham body with non-constant parameters (called non-constant Binghambody).

From the mathematical point of view, this function can describe the accelerated change characteristics of the curve, and its corresponding stress equation is:

$$\sigma = ((1/A)/(1 + 3(B/A)t^2))\varepsilon' + \sigma_s, \tag{2}$$

where A and B are parameters related to viscosity coefficient, so

$$\eta^{\mathrm{B}} = (1/A)/(1 + 3(B/A)t^2), \tag{3}$$

When $t = 0$, $\eta^{\mathrm{B0}} = 1/A$. Furthermore, $H(\sigma)\alpha_{\eta^B} = B/A$. So, the viscosity coefficient (η^{B}) of the Bingham body is calculated as follows:

$$\eta^{\mathrm{B}} = \frac{\eta^{\mathrm{B0}}}{1 + 3H(\sigma)\alpha_{\eta^B}t^2}, \tag{4}$$

$$H(\sigma) = \begin{cases} 0 & \sigma \le \sigma_s \\ \dfrac{\sigma - \sigma_s}{1 - \sigma_s} & \sigma > \sigma_s \end{cases}. \tag{5}$$

where η^{B0} denotes the initial Bingham viscosity coefficient, in units of MPa,$\cdot t$ (t denotes the unit of time); t refers to time, in units of hour, short for h; α_{η^B} is the delay coefficient of the Bingham viscosity coefficient, in units of ($1/t^2$); σ is the stress level applied to rock; and σ_s refers to the stress level corresponding to the long-term rock strength. At the same time, it also represents the threshold value of the stress level when rock begins to exhibit rheological behavior at an accelerated rate. When $\sigma \le \sigma_s$, the stress on the rock is less than the long-term strength and the rock fails to show rheological behavior at an accelerated rate. In this case, the viscosity coefficient of the Bingham body is η^{B0}. When $\sigma > \sigma_s$, the stress on the rock is greater than the long-term strength, and the rock is likely to exhibit rheological behavior at an accelerated rate. In this context, the viscosity coefficient of the Bingham body is η^{B}. In order to determine the influences of time and stress on the viscosity coefficient, the influences of the parameters α_{η^B} and σ on the viscosity coefficient are explored.

For the case of a constant η^{B0} and σ and a changing α_{η^B}, the change in viscosity coefficient η^{B} with time is as displayed in Figure 2. It can be seen that η^{B} decreases with time due to crack propagation. Moreover, the value of the parameter α_{η^B} reflects the rate of decrease of the viscosity coefficient η^{B}. With the increase of α_{η^B}, the attenuation of η^{B} increases.

Under constant η^{B0} and α_{η^B}, the change in viscosity coefficient η^{B} with stress level σ over time is shown in Figure 3. It can be seen that when an instantaneous load is applied to brittle rock, the Bingham viscosity coefficient η^{B0} of the rock is independent of the magnitude of the load, i.e., under different stress levels, brittle rock exhibits the same initial viscosity coefficient. At a certain time after loading, the viscosity coefficient of brittle rock will decrease with increasing stress level and the attenuation rate of the viscosity coefficient of the brittle rock will increase with time. This indicates that the damping of brittle rock subjected to accelerated deformation under high stress decreases.

The one-dimensional constitutive equation of the non-constant Bingham model is as follows:

$$\sigma = \eta^{\mathrm{B}}\varepsilon' + \sigma_{\mathrm{s}} = \frac{\eta^{\mathrm{B0}}}{1 + 3H(\sigma)\alpha_{\eta^B}t^2}\varepsilon' + \sigma_{\mathrm{s}}, \tag{6}$$

where σ_{s} represents long-term strength of rock. The long-term strength is determined by applying a single-stage constant load to the rock at different stress levels until the rock is finally destroyed, and then taking the minimum value of the load that is sufficiently long before the damage as the long-term strength.

Therefore, in a constant stress state, the time-dependent deformation equation of rock can be expressed as follows:

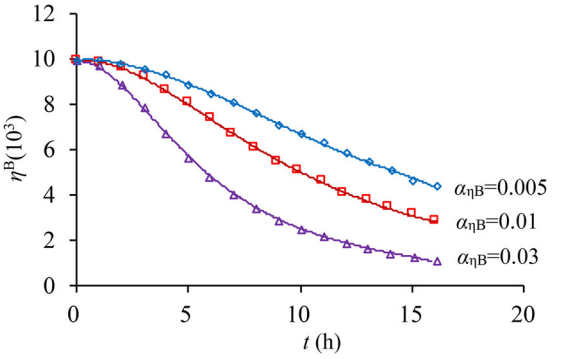

Figure 2. Change in viscosity coefficient with time.

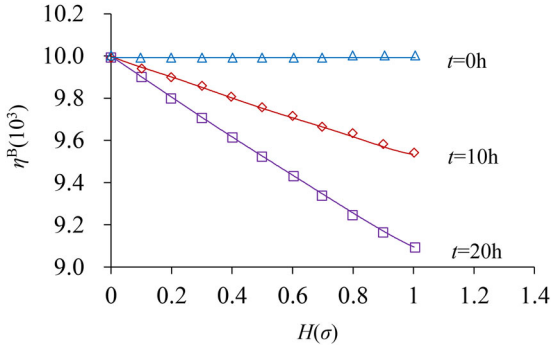

Figure 3. Change in viscosity coefficient with stress.

$$\varepsilon = \frac{t + H(\sigma)\alpha_{\eta^B} t^3}{\eta^{B0}}(\sigma - \sigma_s). \tag{7}$$

Figure 4 shows the effect of the delay coefficient α_{η^B} and initial viscosity coefficient η^{B0} on the time-dependent deformation curve in the acceleration phase. It can be seen that under a given initial strain, when η^{B0} and σ are constant, and α_{η^B} changes independently, the deformation will accelerate as time increases, which fully reflects the nonlinear time-dependent deformation evolution law of the rock. As α_{η^B} increases, the nonlinear characteristics of the time-dependent deformation curve in the acceleration phase becomes more and more pronounced, as shown in Figure 4(a). When α_{η^B} and σ are constant, as the parameter η^{B0} increases, the nonlinear characteristics of the time-dependent deformation curve in the acceleration phase become gradually weaker, and the nonlinear acceleration time-dependent deformation characteristic of the rock becomes less apparent, as shown in Figure 4(b).

3. Viscoelastic-plastic model with non-constant parameters

Through the aforementioned analysis, the non-constant Bingham model is applicable to the description of the viscoplastic behavior of hard brittle rock. In addition to describing the viscoelastic behavior before the accelerated deformation stage, the Burgers viscoelastic model is introduced here. For brittle rock, when the stress on rock masses is greater than a certain value, it mainly exhibits steady-state time-dependent deformation characteristics; when it is less than this value, it exhibits attenuation deformation characteristics. Considering this, a brittle component is introduced to modify the Burgers model (Shen, 2003). The brittle component is primarily used to control the effect of the viscous component in a Maxwell body. Here, we define σ_d as the threshold for the failure of the brittle component. When $\sigma < \sigma_d$, the brittle component plays its role as a rigid body. Moreover, no deformation appears in the loop of the brittle and viscous components and the Maxwell body does not come into effect. Therefore, the Burgers model is simplified into a Kelvin model with three parameters to describe the creep at an attenuated

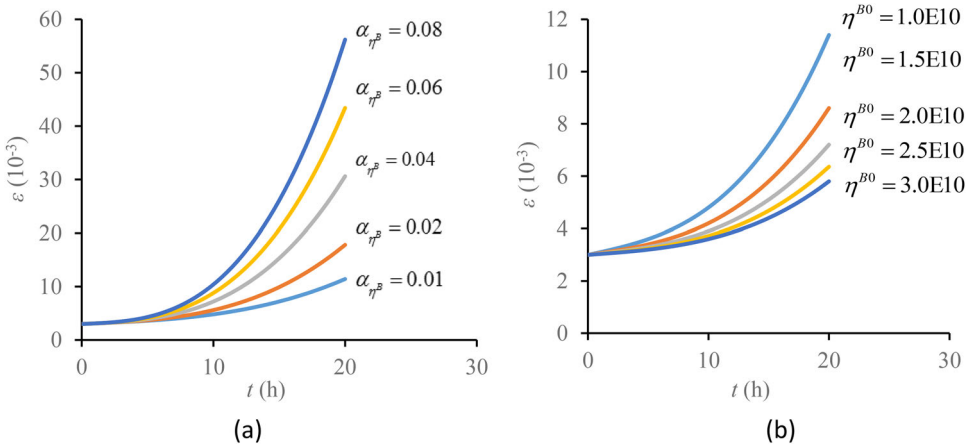

Figure 4. Effects of the delay coefficient and initial viscosity coefficient on the time-dependent deformation curve in the acceleration phase: (a) effect of delay coefficientα_{η^B}; (b) effect of initial viscosity coefficient η^{B0}.

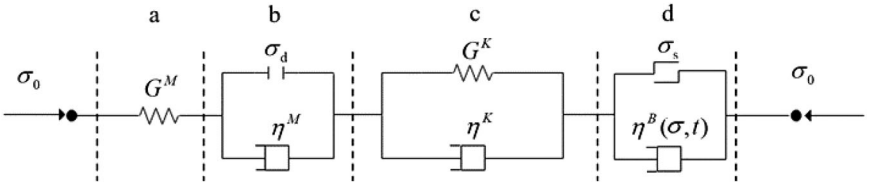

Figure 5. Viscoelastic-plastic model with non-constant parameters (called the non-constant viscoelastic-plastic model below) for brittle rock and related parameters; (a) Maxwell elastic component; (b) visco-brittle body; (c) Kelvin body; (d): Bingham body.

rate. When $\sigma \geq \sigma_d$, the brittle component is fractured and fails and does not bear any stress. The deformation in the loop of the brittle component implies viscous deformation, as shown in component assembly *b* of Figure 5. The viscoelastic model presented here is the Burgers model that considers the stress threshold.

Based on the assumption of a constant bulk modulus, the one-dimensional expression of the conventional Burgers model is given by

$$\varepsilon(t) = \left(\frac{1}{3G^{\mathrm{M}}} + \frac{1}{9K} + \frac{t}{3\eta^{\mathrm{M}}} + \frac{1}{3G^{\mathrm{K}}}\left(1 - \exp\left(-\frac{G^{\mathrm{K}}}{\eta^{\mathrm{K}}}t\right)\right)\right)\sigma_0, \tag{8}$$

where $\varepsilon(\cdot)$ represents the one-dimensional strain; K, G^{M}, η^{M}, G^{K}, and η^{K} are the bulk modulus of the Burgers model, shear modulus of the Maxwell body, viscosity of the Maxwell body, and shear modulus and viscosity coefficient of the Kelvin body, respectively. The three-dimensional (3D) creep model can be expressed as follows:

$$\varepsilon_{ij}(t) = \left(\frac{1}{2G^{\mathrm{M}}} + \frac{t}{2\eta^{\mathrm{M}}} + \frac{1}{2G^{\mathrm{K}}}\left(1 - \exp\left(-\frac{G^{\mathrm{K}}}{\eta^{\mathrm{K}}}t\right)\right)\right)s_{ij} + \frac{1}{9K}\sigma_{kk}\delta_{ij}, \tag{9}$$

where $\varepsilon_{ij}(\cdot)$ represents the 3D strain and δ_{ij} is the Kronecher symbol.

The creep equation of the model in the direction of deviatoric stress is expressed as follows:

$$e_{ij}(t) = \left(\frac{1}{2G^{\mathrm{M}}} + \frac{t}{2\eta^{\mathrm{M}}} + \frac{1}{2G^{\mathrm{K}}}\left(1 - \exp\left(-\frac{G^{\mathrm{K}}}{\eta^{\mathrm{K}}}t\right)\right)\right)s_{ij}, \tag{10}$$

where $e_{ij}(\cdot)$ represents the 3D deviatoric strain and s_{ij} is the component of the 3-D deviatoric strain tensor.

In 3D stress states, the yield approach index (YAI) is adopted to express the variable σ, namely, $\sigma = 1$ – YAI (Zhang et al., 2011). Therefore, the Burgers model considering the stress threshold can be expressed as follows.

When $\sigma = \sigma_d$, Formula (9) is transformed to:

$$\varepsilon_{ij}(t) = \left(\frac{1}{2G^M} + \frac{1}{2G^K}\left(1 - \exp\left(-\frac{G^K}{\eta^K}t\right)\right)\right)s_{ij} + \frac{1}{9K}\sigma_{kk}\delta_{ij}, \tag{11}$$

When $\sigma \geq \sigma_d$, Formula (9) is applied.

By combining the non-constant Bingham model with the Burgers model considering the stress threshold, a new model called the non-constant viscoelastic-plastic model of brittle rock is proposed here, as illustrated in Figure 5. This model can fully describe three-stage, time-dependent mechanical behavior. This model is comprised of four parts: a Maxwell elastic component, a visco-brittle body, a Kelvin body, and a non-constant Bingham body.

1. When $\sigma < \sigma_d$

Under one-dimensional stress states, the one-dimensional stress and strain expressions of the non-constant viscoelastic-plastic model are as follows:

$$\varepsilon = \varepsilon_a + \varepsilon_c, \tag{12}$$

$$\sigma = \sigma_a = \sigma_c, \tag{13}$$

$$\varepsilon_a = \frac{\sigma_a}{G^M} = \frac{\sigma}{G^M}, \tag{14}$$

$$\varepsilon_c = \frac{\sigma_c}{G^K} - \frac{\eta^K}{G^K}\varepsilon'_c = \frac{\sigma}{G^K} - \frac{\eta^K}{G^K}\varepsilon'_c, \tag{15}$$

where σ_a and ε_a refer to the stress and strain on the elastic components in the Maxwell body; σ_c and ε_c denote the stress and strain on the Kelvin body.

Based on Formulae (12)–(15), the constitutive equation of the non-constant viscoelastic-plastic model can be obtained:

$$\frac{\eta^K}{G^K}\varepsilon' + \varepsilon = \frac{\eta^K}{G^M G^K}\sigma' + \frac{G^M + G^K}{G^M G^K}\sigma. \tag{16}$$

(2) When $\sigma_d \leq \sigma < \sigma_s$

The one-dimensional stress and strain expressions of the non-constant viscoelastic-plastic model are as follows:

$$\varepsilon = \varepsilon_a + \varepsilon_b + \varepsilon_c, \tag{17}$$

$$\sigma = \sigma_a = \sigma_b = \sigma_c, \tag{18}$$

where σ_b and ε_b refer to the stress and strain on the visco-brittle body.

It can be also seen that the constitutive equation of the viscous components in a visco-brittle body can be expressed as follows:

$$\eta^M \varepsilon'_b = \sigma_b = \sigma, \tag{19}$$

Therefore, by simultaneously solving Formulae (14) and (15), and (17)–(19), the constitutive equation of the non-constant viscoelastic-plastic model can be attained:

$$\frac{\eta^M \eta^K}{G^K}\varepsilon'' + \eta^M \varepsilon' = \frac{\eta^K \eta^M}{G^M G^K}\sigma'' + \left(\frac{\eta^M G^K + G^M \eta^K + G^M \eta^M}{G^M G^K}\right)\sigma' + \sigma. \tag{20}$$

(3) When $\sigma \geq \sigma_s$

The one-dimensional stress and strain expressions of the non-constant viscoelastic-plastic model are as follows:

$$\varepsilon = \varepsilon_a + \varepsilon_b + \varepsilon_c + \varepsilon_d, \tag{21}$$

$$\sigma = \sigma_a = \sigma_b = \sigma_c = \sigma_d, \tag{22}$$

According to Formulae (10, 14, 15, 19, 21), and (22), it can be seen that:

$$\varepsilon'' + \frac{G^{\mathrm{K}}}{\eta^{\mathrm{K}}}\varepsilon' = \frac{1}{G^{\mathrm{M}}}\sigma'' + \left(\frac{\eta^{\mathrm{M}} + \eta^{\mathrm{K}}}{\eta^{\mathrm{M}}\eta^{\mathrm{K}}} + \frac{G^{\mathrm{K}}}{G^{\mathrm{M}}\eta^{\mathrm{K}}} + \frac{1}{\eta^{\mathrm{B}}}\right)\sigma' + \frac{G^{\mathrm{K}}}{\eta^{\mathrm{M}}\eta^{\mathrm{K}}}\sigma + \left(\frac{G^{\mathrm{K}}}{\eta^{\mathrm{K}}} - \frac{\eta'^{\mathrm{B}}}{\eta^{\mathrm{B}}}\right)\frac{(\sigma - \sigma_s)}{\eta^{\mathrm{B}}}. \tag{23}$$

Overall, the one-dimensional constitutive equation of the non-constant viscoelastic-plastic model for brittle rock is expressed as follows:

$$\begin{cases} \dfrac{\eta^{\mathrm{K}}}{G^{\mathrm{K}}}\varepsilon' + \varepsilon = \dfrac{\eta^{\mathrm{K}}}{G^{\mathrm{M}}G^{\mathrm{K}}}\sigma' + \dfrac{G^{\mathrm{M}} + G^{\mathrm{K}}}{G^{\mathrm{M}}G^{\mathrm{K}}}\sigma, & \sigma < \sigma_{\mathrm{d}} \\ \dfrac{\eta^{\mathrm{M}}\eta^{\mathrm{K}}}{G^{\mathrm{K}}}\varepsilon'' + \eta^{\mathrm{M}}\varepsilon' = \dfrac{\eta^{\mathrm{K}}\eta^{\mathrm{M}}}{G^{\mathrm{M}}G^{\mathrm{K}}}\sigma'' + \\ \left(\dfrac{\eta^{\mathrm{M}}G^{\mathrm{K}} + G^{\mathrm{M}}\eta^{\mathrm{K}} + G^{\mathrm{M}}\eta^{\mathrm{M}}}{G^{\mathrm{M}}G^{\mathrm{K}}}\right)\sigma' + \sigma, & \sigma_{\mathrm{d}} \leq \sigma < \sigma_{\mathrm{s}}, \\ \varepsilon'' + \dfrac{G^{\mathrm{K}}}{\eta^{\mathrm{K}}}\varepsilon' = \dfrac{1}{G^{\mathrm{M}}}\sigma'' + \left(\dfrac{\eta^{\mathrm{M}} + \eta^{\mathrm{K}}}{\eta^{\mathrm{M}}\eta^{\mathrm{K}}} + \dfrac{G^{\mathrm{K}}}{G^{\mathrm{M}}\eta^{\mathrm{K}}} + \dfrac{1}{\eta^{\mathrm{B}}}\right)\sigma' + \\ \dfrac{G^{\mathrm{K}}}{\eta^{\mathrm{M}}\eta^{\mathrm{K}}}\sigma + \left(\dfrac{G^{\mathrm{K}}}{\eta^{\mathrm{K}}} - \dfrac{\eta'^{\mathrm{B}}}{\eta^{\mathrm{B}}}\right)\dfrac{(\sigma - \sigma_{\mathrm{s}})}{\eta^{\mathrm{B}}}, & \sigma \geq \sigma_{\mathrm{s}} \end{cases} \tag{24}$$

It is worth noting that ε in the aforementioned formulae refers to the strain, excluding the component of strain generated due to the bulk modulus, i.e., $\varepsilon = \varepsilon^* - \sigma/(9K)$, where, ε^* represents the total strain. To calculate the total strain, the strain generated due to the bulk modulus should be added. Therefore, ε is replaced with the component e_{ij} of the deviatoric strain tensor, while the component s_{ij} of the deviatoric strain tensor is used to replace σ. By combining the volumetric strain ε_m calculated from the volumetric stress σ_m, i.e., $\varepsilon_m = \sigma_m/(3K)$, the constitutive equation in a 3D stress state can be obtained:

$$\begin{cases} \dfrac{\eta^{\mathrm{K}}}{G^{\mathrm{K}}}e'_{ij} + e_{ij} = \dfrac{\eta^{\mathrm{K}}}{G^{\mathrm{M}}G^{\mathrm{K}}}s'_{ij} + \dfrac{G^{\mathrm{M}} + G^{\mathrm{K}}}{G^{\mathrm{M}}G^{\mathrm{K}}}s_{ij}, & \sigma < \sigma_{\mathrm{d}} \\ \dfrac{\eta^{\mathrm{M}}\eta^{\mathrm{K}}}{G^{\mathrm{K}}}e''_{ij} + \eta^{\mathrm{M}}e'_{ij} = \dfrac{\eta^{\mathrm{K}}\eta^{\mathrm{M}}}{G^{\mathrm{M}}G^{\mathrm{K}}}s''_{ij} + \left(\dfrac{\eta^{\mathrm{M}}G^{\mathrm{K}} + G^{\mathrm{M}}\eta^{\mathrm{K}} + G^{\mathrm{M}}\eta^{\mathrm{M}}}{G^{\mathrm{M}}G^{\mathrm{K}}}\right)s'_{ij} + s_{ij}, & \sigma_{\mathrm{d}} \leq \sigma < \sigma_{\mathrm{s}} \\ e''_{ij} + \dfrac{G^{\mathrm{K}}}{\eta^{\mathrm{K}}}e'_{ij} = \dfrac{1}{G^{\mathrm{M}}}s''_{ij} + \left(\dfrac{\eta^{\mathrm{M}} + \eta^{\mathrm{K}}}{\eta^{\mathrm{M}}\eta^{\mathrm{K}}} + \dfrac{G^{\mathrm{K}}}{G^{\mathrm{M}}\eta^{\mathrm{K}}} + \dfrac{1}{\eta^{\mathrm{B}}}\right)s'_{ij} + \dfrac{G^{\mathrm{K}}}{\eta^{\mathrm{M}}\eta^{\mathrm{K}}}s_{ij} + \left(\dfrac{G^{\mathrm{K}}}{\eta^{\mathrm{K}}} - \dfrac{\eta'^{\mathrm{B}}}{\eta^{\mathrm{B}}}\right)\dfrac{(s_{ij} - \sigma_{\mathrm{s}})}{\eta^{\mathrm{B}}}, & \sigma \geq \sigma_{\mathrm{s}} \\ \varepsilon_{\mathrm{m}} = \dfrac{\sigma_{\mathrm{m}}}{3K} \end{cases} \tag{25}$$

4. Non-constant viscoelastic-plastic creep equation

Under the creep condition, the load applied to the rock remains constant, i.e., $\sigma = \sigma_0$. When $\sigma_0 < \sigma_{\mathrm{d}}$, $\varepsilon(t) = 0$ at $t = 0$; therefore, the integral is carried out based on the first equation of Formula (24) and the part of the strain generated due to the bulk modulus is taken into account. In this way, Formula (26) can be obtained:

$$\varepsilon(t) = \frac{\sigma_0}{9K} + \frac{\sigma_0}{3G^M} + \frac{\sigma_0}{3G^K}\left(1 - \exp\left(-\frac{G^K}{\eta^K}t\right)\right). \tag{26}$$

Differentiating twice on both sides of Formula (26) yields

$$\varepsilon'(t) = \frac{\sigma_0}{3\eta^{\mathrm{K}}}\exp\left(-\frac{G^{\mathrm{K}}}{\eta^{\mathrm{K}}}t\right), \tag{27}$$

$$\varepsilon''(t) = -\frac{G^{\mathrm{K}}}{3(\eta^{\mathrm{K}})^2}\exp\left(-\frac{G^{\mathrm{K}}}{\eta^{\mathrm{K}}}t\right)\sigma_0. \tag{28}$$

It can be seen from Formulae (27) and (28) that at the creep rate of $\varepsilon' \geq 0$ and the creep acceleration of $\varepsilon'' \leq 0$, the model is subjected to instantaneous elastic deformation $(\sigma_0/(9K) + \sigma_0/(3G^M))$ (instantaneous elastic recovery strain under unloading) and creep deformation under increasing loading) $(\sigma_0/(3G^K)[1-\exp(-G^K t/\eta^K)])$ (elastic after-effect strain under unloading). On the condition that time tends to infinity, the final deformation of materials shows a fixed value $(\sigma_0/(9K) + \sigma_0/(3G^M) + \sigma_0/(3G^K))$. In this case, deformation is unrelated to time, i.e., the system tends toward stable deformation. Additionally, with time, the creep rate ε' constantly declines from $\sigma_0/(3\eta^K)$, and when time approaches infinity $\varepsilon'(\infty) = 0$. Additionally, the creep acceleration ε'' constantly increases from $-G^K\sigma_0/3(\eta^K)^2$ with time, eventually becoming $\varepsilon''(\infty) = 0$. Therefore, the creep equation of the model is simplified into the creep equation of the Kelvin model to describe the characteristics of viscoelastic creep of brittle rock at an attenuated rate, i.e., the creep deformation reflected by the model is stable.

When $\sigma_{\mathrm{d}} \leq \sigma_0 < \sigma_{\mathrm{s}}$, Formula (29) can be obtained through the Laplace transform:

$$\varepsilon(t) = \frac{\sigma_0}{9K} + \frac{\sigma_0}{3G^{\mathrm{M}}} + \frac{\sigma_0}{3\eta^{\mathrm{M}}}t + \frac{\sigma_0}{3G^{\mathrm{K}}}\left(1 - \exp\left(-\frac{G^{\mathrm{K}}}{\eta^{\mathrm{K}}}t\right)\right). \tag{29}$$

Differentiating both sides of Formula (29) twice yields

$$\varepsilon'(t) = \frac{\sigma_0}{3\eta^{\mathrm{M}}} + \frac{\sigma_0}{3\eta^{\mathrm{K}}}\exp\left(-\frac{G^{\mathrm{K}}}{\eta^{\mathrm{K}}}t\right), \tag{30}$$

$$\varepsilon''(t) = -\frac{G^{\mathrm{K}}}{3(\eta^{\mathrm{K}})^2}\exp\left(-\frac{G^{\mathrm{K}}}{\eta^{\mathrm{K}}}t\right)\sigma_0. \tag{31}$$

Based on Formulae (30) and (31), the creep rate is $\varepsilon' > 0$, while the creep acceleration is $\varepsilon'' \leq 0$. In this context, the creep rate ε' constantly decreases from $(\sigma_0/(3\eta^M) + \sigma_0/(3\eta^K))$ with time. When time approaches infinity, $\varepsilon'(\infty) = \sigma_0/(3\eta^M)$, i.e., the final creep rate of the model is stable. Additionally, the creep acceleration ε'' constantly rises from $-G^K\sigma_0/(3(\eta^K)^2)$ with time, eventually becoming $\varepsilon''(\infty) = 0$. In this case, the creep equation of the model is equivalent to that of the Burgers model, which is used to describe the characteristics of the viscoelastic steady creep of brittle rock, i.e., the model reflects metastable creep deformation.

On the condition that the applied constant stress is $\sigma_0 \geq \sigma_{\mathrm{s}}$, Formula (32) can be obtained through the Laplace transform:

$$\varepsilon(t) = \frac{\sigma_0}{9K} + \frac{\sigma_0}{3G^{\mathrm{M}}} + \frac{\sigma_0}{3\eta^{\mathrm{M}}}t + \frac{\sigma_0}{3G^{\mathrm{K}}}\left(1 - \exp\left(-\frac{G^{\mathrm{K}}}{\eta^{\mathrm{K}}}t\right)\right) + \frac{t + H(\sigma_0)\alpha_{\eta^{\mathrm{B}}}t^3}{\eta^{\mathrm{B0}}}(\sigma_0 - \sigma_{\mathrm{s}}). \tag{32}$$

Differentiating both sides of Formula (32) yields

$$\varepsilon'(t) = \frac{\sigma_0}{3\eta^{\mathrm{M}}} + \frac{\sigma_0}{3\eta^{\mathrm{K}}}\exp\left(-\frac{G^{\mathrm{K}}}{\eta^{\mathrm{K}}}t\right) + \frac{1 + 3H(\sigma_0)\alpha_{\eta^{\mathrm{B}}}t^2}{\eta^{\mathrm{B0}}}(\sigma_0 - \sigma_{\mathrm{s}}), \tag{33}$$

$$\varepsilon''(t) = -\frac{G^{\mathrm{K}}}{3(\eta^{\mathrm{K}})^2}\exp\left(-\frac{G^{\mathrm{K}}}{\eta^{\mathrm{K}}}t\right)\sigma_0 + \frac{6H(\sigma_0)\alpha_{\eta^{\mathrm{B}}}t}{\eta^{\mathrm{B0}}}(\sigma_0 - \sigma_{\mathrm{s}}). \tag{34}$$

It can be seen from Formulae (33) and (34) that when $H(\sigma_0) = 0$ or $\alpha_{\eta^B} = 0$, the creep rate is $\varepsilon' > 0$, while the creep acceleration is $\varepsilon'' \leq 0$. According to the aforementioned analysis, it can be seen that in that

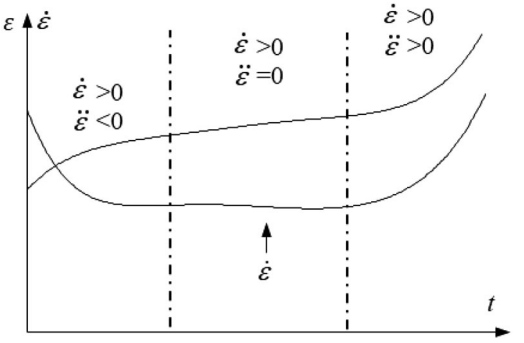

Figure 6. Creep characteristics of the viscoelastic-plastic rheological model.

case the model describes initial and steady-state creep. When $H(\sigma_0) \neq 0$ and $\alpha_{\eta^B} \neq 0$, the creep rate is $\varepsilon' > 0$ while ε'' is probably less than, equal to, or greater than 0, i.e., in this context, the model can describe the 3 complete stages of creep, including initial creep, steady-state creep, and accelerated creep, as shown in Figure 6. As can be seen from Figure 6, this model can well describe the full-stage creep characteristics of hard brittle rock under high stress, especially non-constant Newtonian body is added to effectively describe the characteristics of the accelerated creep phase.

Thus, Formulae (26, 29), and (32) constitute the creep equation under a one-dimensional stress state. The 3-D creep equation of the non-constant viscoelastic-plastic model for brittle rock becomes

$$\varepsilon_{ij}(t) = \begin{cases} \left(\dfrac{1}{2G^{\mathrm{M}}} + \dfrac{1}{2G^{\mathrm{K}}}\left(1 - \exp\left(-\dfrac{G^{\mathrm{K}}}{\eta^{\mathrm{K}}}t\right)\right)\right)(s_{ij})_0 + \dfrac{1}{9K}(\sigma_{kk})_0\delta_{ij}, & \sigma < \sigma_{\mathrm{d}} \\ \left(\dfrac{1}{2G^{\mathrm{M}}} + \dfrac{t}{2\eta^{\mathrm{M}}} + \dfrac{1}{2G^{\mathrm{K}}}\left(1 - \exp\left(-\dfrac{G^{\mathrm{K}}}{\eta^{\mathrm{K}}}t\right)\right)\right)(s_{ij})_0 + \\ \dfrac{1}{9K}(\sigma_{kk})_0\delta_{ij}, & \sigma_{\mathrm{d}} \leq \sigma < \sigma_{\mathrm{s}} \\ \left(\dfrac{1}{2G^{\mathrm{M}}} + \dfrac{t}{2\eta^{\mathrm{M}}} + \dfrac{1}{2G^{\mathrm{K}}}\left(1 - \exp\left(-\dfrac{G^{\mathrm{K}}}{\eta^{\mathrm{K}}}t\right)\right)\right)(s_{ij})_0 + \\ \dfrac{t + H(\sigma_0)\alpha_{\eta^B}t^3}{\eta^{B0}}((s_{ij})_0 - \sigma_s) + \dfrac{1}{9K}(\sigma_{kk})_0\delta_{ij}, & \sigma \geq \sigma_{\mathrm{s}} \end{cases} \tag{35}$$

where σ_0 refers to the stress level in the 3D stress state.

5. Non-constant viscoelastic-plastic relaxation equation

Based on the assumption of a constant bulk modulus, the stress generated due to the bulk modulus is not taken into account during the analysis of the relaxation equation in this and subsequent sections. For the non-constant viscoelastic-plastic model for brittle rock, when $\sigma_0 < \sigma_{\mathrm{d}}$, the constant strain $\varepsilon = \varepsilon_0$ is applied, i.e., $\varepsilon'(t) = 0$, and therefore $\sigma = \sigma_0$ at $t = 0$. Subsequently, the condition is substituted into the first equation in Formula (24) and Laplace transformation is carried out. Based on the Laplace normal transform, it can be seen that

$$\frac{\varepsilon_0}{s} = P_1(\bar{\sigma} - \sigma_0) + P_0\bar{\sigma}, \tag{36}$$

$$P_0 = \frac{G^{\mathrm{M}} + G^{\mathrm{K}}}{G^{\mathrm{M}}G^{\mathrm{K}}}, \tag{37}$$

$$P_1 = \frac{\eta^{\mathrm{K}}}{G^{\mathrm{M}}G^{\mathrm{K}}}, \tag{38}$$

where $\bar{\sigma}$ refers to the Laplace transform function of stress and s refers to the variable in the image function of the Laplace transform.

By calculating the aforementioned formulae, Formula (37) can be acquired:

$$\bar{\sigma} = \frac{\varepsilon_0}{P_1 s^2 + P_0 s} + \frac{P_1}{P_1 s + P_0}\sigma_0 = \left(\frac{1}{s(s + P_0/P_1)}\right)\frac{\varepsilon_0}{P_1} + \left(\frac{1}{s + P_0/P_1}\right)\sigma_0. \tag{39}$$

Inverse Laplace transformation of Formula (39) gives

$$L^{-1}\left(\frac{1}{s(s + P_0/P_1)}\right) = \frac{P_1}{P_0}\left(1 - \exp\left(-\frac{P_0}{P_1}t\right)\right), \tag{40}$$

$$L^{-1}\left(\frac{1}{s + P_0/P_1}\right) = \exp\left(-\frac{P_0}{P_1}t\right), \tag{41}$$

where $L^{-1}(\cdot)$ expresses the inverse Laplace transform.

Therefore, the relaxation equation in that stress state can be obtained:

$$\sigma(t) = \frac{\varepsilon_0}{P_0} + \left(\sigma_0 - \frac{\varepsilon_0}{P_0}\right)\exp\left(-\frac{P_0}{P_1}t\right). \tag{42}$$

Substituting P_0 and P_1 into Formula (42) yields

$$\sigma(t) = \frac{G^{\mathrm{M}}G^{\mathrm{K}}}{G^{\mathrm{M}} + G^{\mathrm{K}}}\varepsilon_0 + \left(\sigma_0 - \frac{G^{\mathrm{M}}G^{\mathrm{K}}}{G^{\mathrm{M}} + G^{\mathrm{K}}}\varepsilon_0\right)\exp\left(-\frac{G^{\mathrm{M}} + G^{\mathrm{K}}}{\eta^{\mathrm{K}}}t\right). \tag{43}$$

The stress relaxation of the model equation begins at σ_0, progressively decreases with time in a negative exponential manner, and finally stabilizes at a constant value, i.e., $G^{\mathrm{M}}G^{\mathrm{K}}\varepsilon_0/(G^{\mathrm{M}} + G^{\mathrm{K}})$. It is worth noting that the stress induced by the bulk modulus is not considered, i.e., $\sigma_0 = \sigma^* - 9K\varepsilon_0$, where σ^* refers to the total stress. In this case, the stress finally relaxes to $(G^{\mathrm{M}}G^{\mathrm{K}}\varepsilon_0/(G^{\mathrm{M}} + G^{\mathrm{K}}) + 9K\varepsilon_0)$.

When $\sigma_{\mathrm{d}} \le \sigma_0 < \sigma_s$, the constant strain $\varepsilon = \varepsilon_0$ is applied, i.e., $\varepsilon'(t) = \varepsilon''(t) = 0$, so that $\sigma = \sigma_0$ and $\sigma'(t) = \sigma''(t) = 0$ at $t = 0$. Substituting this condition into the second equation in Formula (24) and conducting Laplace normal transformation yields

$$\varepsilon_0(q_1 + q_2 s) = \bar{\sigma}(1 + P_1 s + P_2 s^2), \tag{44}$$

$$P_1 = \frac{\eta^{\mathrm{M}}G^{\mathrm{K}} + G^{\mathrm{M}}\eta^{\mathrm{K}} + G^{\mathrm{M}}\eta^{\mathrm{M}}}{G^{\mathrm{M}}G^{\mathrm{K}}}, \tag{45}$$

$$P_2 = \frac{\eta^{\mathrm{K}}\eta^{\mathrm{M}}}{G^{\mathrm{M}}G^{\mathrm{K}}}, \tag{46}$$

$$q_1 = \eta^{\mathrm{M}}, \tag{47}$$

$$q_2 = \frac{\eta^{\mathrm{M}}\eta^{\mathrm{K}}}{G^{\mathrm{K}}}. \tag{48}$$

By simultaneously calculating the above formulae, the following can be derived:

$$\begin{aligned}\bar{\sigma} = \frac{q_1 + q_2 s}{1 + P_1 s + P_2 s^2}\varepsilon_0 &= \frac{q_1}{1 + P_1 s + P_2 s^2} + \frac{q_2 s}{1 + P_1 s + P_2 s^2} \\ &= \frac{1}{P_2}\left(\frac{q_1}{(s + \alpha)(s + \beta)} + \frac{q_2 s}{(s + \alpha)(s + \beta)}\right)\end{aligned}, \tag{49}$$

$$1 + P_1 s + P_2 s^2 = (s + \alpha)(s + \beta)P_2, \tag{50}$$

$$\alpha = \frac{1}{2P_2}(P_1 + \sqrt{P_1^2 - 4P_2}), \tag{51}$$

$$\beta = \frac{1}{2P_2}(P_1 - \sqrt{P_1^2 - 4P_2}). \tag{52}$$

Inverse Laplace transformation of Formula (49) yields

$$L^{-1}\left(\frac{1}{(s + \alpha)(s + \beta)}\right) = \frac{1}{-\alpha + \beta}(e^{-\alpha t} - e^{-\beta t}), \tag{53}$$

Table 1. Mechanical parameters for the numerical simulation test.

C_{pea} (MPa)	C_{res} (MPa)	$\varepsilon^{p}_{v,c}$	ϕ_{pea} (°)	ϕ_{res} (°)	$\varepsilon^{p}_{v,\phi 1}$	$\varepsilon^{p}_{v,\phi 2}$	$\varepsilon^{p}_{v,\psi}$	Tensile strength (MPa)
13.57	2.55	1.5e-3	50	40	1.5e-3	3.0e-3	5.1e-2	1.5

$$L^{-1}\left(\frac{s}{(s+\alpha)(s+\beta)}\right)=\frac{1}{-\alpha+\beta}(-\alpha e^{-\alpha t}+\beta e^{-\beta t}), \tag{54}$$

Therefore, the relaxation equation in the stress state can be obtained:

$$\sigma(t)=\frac{\varepsilon_0}{\beta-\alpha}\left((-q_1+\alpha q_2)e^{-\alpha t}+(q_1-\beta q_2)e^{-\beta t}\right). \tag{55}$$

By substituting the values of α and β, the following formulae are obtained:

$$\sigma(t)=\frac{\varepsilon_0}{\sqrt{P_1^2-4P_2}}\left(\left(-q_1+\frac{P_1+\sqrt{P_1^2-4P_2}}{2P_2}q_2\right)\exp\left(-\frac{P_1+\sqrt{P_1^2-4P_2}}{2P_2}t\right)\right.$$
$$\left.+\left(q_1-\frac{P_1-\sqrt{P_1^2-4P_2}}{2P_2}q_2\right)\exp\left(-\frac{P_1-\sqrt{P_1^2-4P_2}}{2P_2}t\right)\right). \tag{56}$$

where the expressions of P_1, P_2, q_1, and q_2 are shown in Formulae (45)–(48).

According to Formula (56), $\sigma_0=q_2\varepsilon_0/P_2=G^{K}\varepsilon_0$, which is the initial stress at $t=0$. It is worth noting that the stress borne by the bulk modulus is not taken into account, i.e., $\sigma_0=\sigma^{*}-9K\varepsilon_0$, where σ^{*} refers to the total stress. It can also be seen that if the stress borne by bulk modulus is considered, the stress relaxation is nearly equivalent to $(9K\varepsilon_0)$ over time.

When $\sigma_0\geq\sigma_s$, the applied constant strain $\varepsilon=\varepsilon_0$, i.e., $\varepsilon'(t)=\varepsilon''(t)=0$, and therefore$\sigma=\sigma_0$ and $\sigma'(0)=0$ at $t=0$. By substituting this condition into the third equation of Formula (24) and performing Laplace transformation according to the aforementioned method, the relaxation equation at that stress state can be acquired. Additionally, it can be seen that, over time, the stress relaxation is nearly equivalent to $(9K\varepsilon_0+\sigma_s)$, i.e., incomplete relaxation, which conforms to the characteristics of the rock materials themselves. In a 3D stress state, the result can be deduced using a similar method based on the 3D constitutive equation.

6. Model suitability test

In this study, the ability of the non-constant viscoelastic-plastic model to describe the time-dependent deformation of hard brittle rock was tested based on the creep test results of Jinping marble. In the model verification, the elastoplastic mechanical behavior of hard and brittle marble is described by the hardening-softening constitutive model proposed by Huang et al. (2020). The elastoplastic mechanical parameters of marble are shown in Table 1. The mechanical parameters of this model were first identified. Then, the step-by step loading numerical simulation test was conducted to obtain the curves of the various stages of the time-dependent deformation of the marble, which could then be used to test the ability of the model to describe the time-dependent deformation characteristics of rock under different stress conditions.

In Table 1, C_{pea}, C_{res}, $\varepsilon^{p}_{v,c}$, ϕ_{pea}, ϕ_{res}, $\varepsilon^{p}_{v,\phi 1}$, $\varepsilon^{p}_{v,\phi 2}$, $\varepsilon^{p}_{v,\psi}$ represent the peak cohesive stress, the residual cohesive stress, the plastic volume strain corresponding to the starting point of residual cohesive stress, the peak internal friction angle, the residual internal friction angle, the plastic volume strain corresponding to peak internal friction angle, the plastic volume strain corresponding to the residual internal friction angle, and the plastic volume strain corresponding to the peak expansion angle, respectively.

By using the non-linear least squares method based on the Levenberg-Marquardt (LM) algorithm, the parameters of the proposed model were identified. This technique combines the Gauss-Newton method and the gradient descent algorithm, thereby exhibiting the rapid convergence of the Gauss-Newton method while overcoming the drawbacks of Newton's method, i.e., failure to effectively overcome singular and non-positive definite matrices and having a strict requirement on initial point selection. Additionally, the combined approach also exhibits the global searching characteristic of the gradient descent algorithm, whose search velocity is faster than that of the gradient method owing to the application

Table 2. Results of parameter identification for the viscoelastic-plastic NRCM for marble.

Confining pressure (MPa)	Pore water pressure (MPa)	Stress level (MPa)	K (GPa)	G^{M} (GPa)	G^{K} (GPa)	η^{M} (GPa·h)	η^{K} (GPa·h)	η^{B0} (GPa·h)	$\alpha_{\eta B}$ ($1/h^2$)	Residual sum of squares ($\times 10^{-8}$)	Correlation coefficient R
15	0	51	6.59	4.34	26.15	30,711.42	60.10	–	–	5.36	0.96
		73	10.81	7.12	5.31	3407.05	12.32	–	–	4.18	0.99
		99	8.28	5.45	2.05	3226.19	0.33	866.37	0.53	7.73	0.99
Mean			8.56	5.64	11.17	12,448.22	24.25	866.37	0.53	–	–
15	5	35	3.84	2.53	8.10	6150.71	112.93	–	–	15.66	0.98
		55	7.97	5.25	17.09	4286.69	103.81	–	–	2.25	0.99
		73	5.88	3.87	13.95	3394.82	79.17	–	–	2.05	0.99
Mean			5.90	3.88	13.05	4610.74	98.64	–	–	–	–
25	5	48	6.71	4.42	69.57	32,794.95	56.35	–	–	0.97	0.96
		83	10.94	7.20	15.98	7711.46	22.52	–	–	4.26	0.99
		111	8.29	5.46	6.90	55,36.78	27.58	–	–	103.32	0.98
Mean			8.65	5.69	30.82	15,347.73	35.48	–	–	–	–
35	5	65	9.52	6.27	45.65	8226.91	262.38	–	–	1.90	0.98
		100	12.57	8.28	25.69	6082.43	86.26	–	–	9.11	0.97
		130	12.45	8.20	14.49	6222.39	70.25	–	–	10.26	0.98
Mean			11.51	7.58	28.61	6843.91	139.63	–	–	–	–

of approximate second-order derivative information. Moreover, in this method, fewer parameters need to be adjusted, thus avoiding the influence of human factors to some extent. Therefore, this method demonstrates superiority in identifying parameters.

For rheological tests under multi-stage loading, the total load can be expressed as $\sigma = \sum_{m=1}^{N} \Delta\sigma_m$. According to the Boltzmann superposition principle, the strain $\varepsilon_t(X)$ at time t can be calculated as follows:

$$\varepsilon_t(X) = \sum_{m=1}^{N} \Delta\sigma_m J(t - t_m), \tag{57}$$

where X represents the parameter vector of the rheological model and $\Delta\sigma_m$ denotes the stress increment ($\Delta\sigma_1 = \sigma_1$, at the first-stage load) for the mth load. Moreover, $J(t-t_m)$, t_m, and N represent the creep compliance related to the parametric variable X, the starting time of the mth load, and the times of multi-stage loading at t, respectively. The objective function for identifying parameters can be calculated according to the following formula:

$$f_{ij}(X) = \sum_{t=t_0}^{t_T} [\varepsilon_t(X) - \varepsilon^{\exp}(t)]^2. \tag{58}$$

where $\varepsilon^{\exp}(t)$ and t_T represent the test value and total duration of the rheological test, respectively.

Based on the aforementioned objective function, the repeated iterative optimization was carried out using the LM algorithm for parameter identification until the objective function satisfied the preset allowable error limit. In this context, the calculation was ended to acquire the parameters.

Here, the results of the graded loading creep test for Jinping marble were adopted. Pore pressure was also applied in this test, but no matter how the pore water pressure affects the rheological mechanical properties of the rock, it has no effect on the rheological mechanical parameters of marble under different conditions.

Based on the results of the creep test under multi-stage loading, the creep parameters obtained under multi-stage loads were separately obtained and then averaged. The acquired creep parameters are listed in Table 2. It can be seen that the rheological parameters acquired based on different rock samples showed certain discrete properties while generally exhibiting a certain regularity. Under the same water pressure, the instantaneous elastic parameters K and G^{M} increased with confining pressure. Moreover, η^{M} also increased with confining pressure, while delay time ($\tau = \eta^{K}/(G^{K})$) decreased with increasing confining pressure. These results indicate that the rheological capacity of brittle rock weakens with increasing confining pressure.

Figure 7 shows the comparison of the calculated and experimental values of the time-dependent deformation of marble. It can be seen that the calculated results agree well with the test results. The

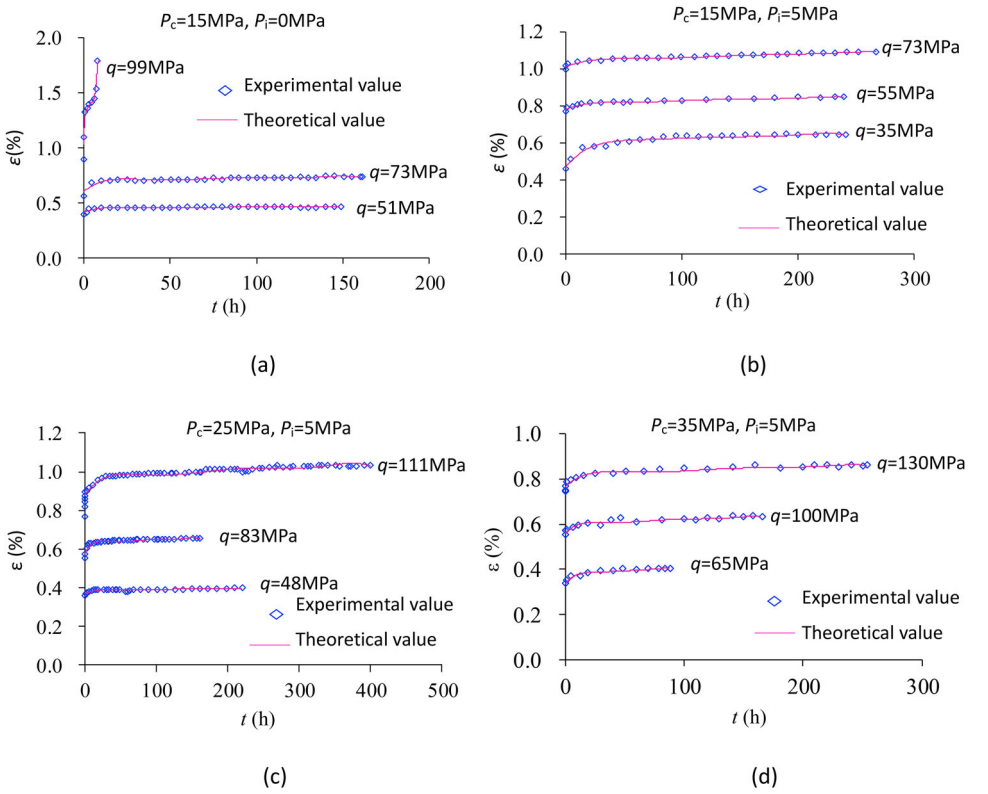

Figure 7. Comparison between the values obtained from the creep testing of marble and those from theoretical analysis: (a) P_c = 15 MPa, P_i = 0 MPa; (b) P_c = 15 MPa, P_i = 5 MPa; (c) P_c = 25 MPa, P_i = 5 MPa; (d) P_c = 35 MPa, P_i = 5 MPa (P_c is confining pressure; P_i is pore water pressure).

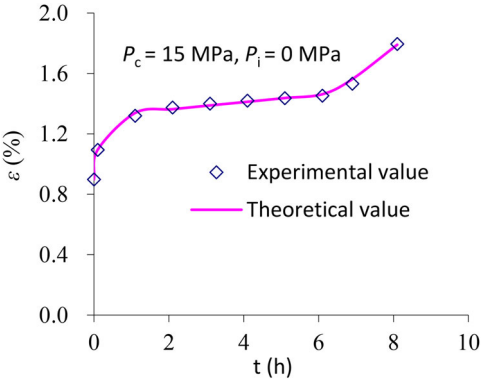

Figure 8. Comparison of test results with theoretical values at q = 99 MPa in Figure 7(a).

maximum and minimum of the residual sums of squares were 1.03×10^{-6} and 0.97×10^{-8}, respectively, with correlation coefficients never less than 0.96. Figure 8 is the evolution curve of deformation with time at q = 99 MPa in Figure 7(a). The comparison of the theoretical and experimental values reveals that the proposed model can describe the evolutionary characteristics of the three stages of time-dependent deformation, i.e., initial attenuation, steady state, and accelerated time-dependent deformation.

Based on the mechanical parameters in Tables 1 and 2, a creep simulation test under multi-stage loading was carried out on a cylindrical sample (diameter, 50 mm; height, 100 mm). We assigned 100.7 GPa·h to η^{B0}, 0.01/h^2 to $\alpha_{\eta B}$. During testing, a confining pressure of 10 MPa was imposed and an axial load was

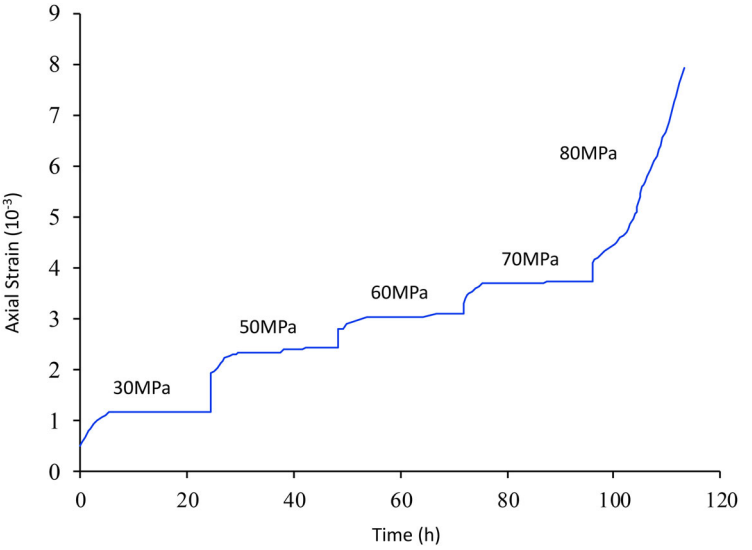

Figure 9. Changes in axial strain of the cylindrical sample with time under different axial loads calculated by the non-constant viscoelastic-plastic model (data on the curve refer to axial load).

applied in a stepwise fashion, at 30, 50, 60, 70, and 80 MPa. The creep stage lasted for 24 h under each load, until the rock sample was damaged at an accelerated rate. Figure 9 shows the evolution axial strain curve of the sample with time under different axial loads (as simulated). It can be seen that the proposed model can reasonably describe the nonlinear rheological characteristics of brittle rock.

7. Conclusions

The deep underground engineering work required during large construction projects is undertaken in a high geostress environment over an extended period of time, resulting in increasingly significant problems concerning the operational safety of engineering caused by the long-term mechanical responses of the surrounding rock. To describe the rheological mechanical behavior of brittle rock under high geostress, a non-constant viscoelastic-plastic model was proposed. The following conclusions are drawn:

1. The rheological mechanical behavior of hard brittle rock is related to the stress conditions. To describe the influence of stress conditions on the viscoplastic behavior of rock, a non-constant Newtonian fluid taking into consideration the influence of stress state was proposed. Moreover, the relationship between the viscosity coefficient of the non-constant Bingham body and stress level was established. Analysis revealed that the viscosity coefficient decreases with time, reflecting the law that the viscosity coefficient of rock gradually decreases due to crack propagation. The viscosity coefficient decreases with increasing stress level, a finding that can be used to describe the development of deformation in brittle rock at an accelerated rate under the effect of high stress. The nonlinear characteristics of the time-dependent deformation curves of rock become more and more significant with increasing viscosity coefficient. As the initial viscosity coefficient increases, the nonlinear characteristics of the acceleration phase of the time-dependent deformation curve become less and less obvious.
2. Under lower stress, brittle rock rapidly changes to an attenuated time-dependent deformation stage after the initial stage. Steady-state time-dependent deformation behavior is only exhibited under higher stress conditions. The proposed non-constant viscoelastic-plastic constitutive model can well describe the attenuation behavior and steady-state behavior of rock under different stress conditions.

Notation

ε strain
ε' creep rate

ε'' creep acceleration
ε^* total strain
ε_0 initial strain at $t = 0$
ε_a strain on the elastic components in the Maxwell body
ε_b strain on the visco-brittle body.
ε_c strain on the Kelvin body.
ε_m volumetric strain
σ stress
σ' stress rate
σ'' stress acceleration
σ^* total stress
σ_s long-term rock strength
σ_0 initial stress at $t = 0$
σ_a stress on the elastic components in the Maxwell body
σ_b stress on the visco-brittle body
σ_c stress on the Kelvin body
σ_d threshold for the failure of the brittle component
σ_a stress on the elastic components in the Maxwell body
σ_b stress on the visco-brittle body
σ_m volumetric stress
$\bar{\sigma}$ Laplace transform function of stress
t time
A parameters related to viscosity coefficient, $\eta^{B0} = 1/A$
B parameters related to viscosity coefficient, $H(\sigma)\alpha_{\eta^B} = B/A$
η^B viscosity coefficient of the Bingham body when $\sigma > \sigma s$
η^{B0} viscosity coefficient of the Bingham body when $\sigma \leq \sigma s$
η^M viscosity coefficient of the Maxwell body
η^K viscosity coefficient of the Kelvin body
$H(\sigma)$ $H(\sigma) = \begin{cases} 0 & \sigma \leq \sigma_s \\ \dfrac{\sigma - \sigma_s}{1 - \sigma_s} & \sigma > \sigma_s \end{cases}$
α_{η^B} the delay coefficient of the Bingham viscosity coefficient
G^M shear modulus of the Maxwell body
G^K shear modulus of the Kelvin body
K bulk modulus of the Burgers model
ε_{ij} strain tensor in three-dimensional coordinate system
s_{ij} the component of the 3D deviatoric strain tensor
σ_{kk} stress tensor invariant
δ_{ij} Kronecker Delta
e_{ij} the 3D deviatoric strain
P_1 $P_1 = \frac{\eta^M G^K + G^M \eta^K + G^M \eta^M}{G^M G^K}$
P_2 $P_2 = \frac{\eta^K \eta^M}{G^M G^K} P_0 P_0 = \frac{G^M + G^K}{G^M G^K}$
s variable in the image function of the Laplace transform
$L^{-1}(\cdot)$ inverse Laplace transform
q_1 $q_1 = \eta^M$
q_2 $q_2 = \frac{\eta^M \eta^K}{G^K}$
α $\alpha = \frac{1}{2P_2}\left(P_1 + \sqrt{P_1^2 - 4P_2}\right)$
β $\beta = \frac{1}{2P_2}\left(P_1 - \sqrt{P_1^2 - 4P_2}\right)$
e natural logarithm in Laplace transform

C_{pea}	peak cohesive stress
C_{res}	residual cohesive stress
$\varepsilon_{v,c}^{p}$	plastic volume strain corresponding to the starting point of residual cohesive stress
ϕ_{pea}	peak internal friction angle
ϕ_{res}	residual internal friction angle
$\varepsilon_{v,\phi 1}^{p}$	plastic volume strain corresponding to peak internal friction angle
$\varepsilon_{v,\phi 2}^{p}$	plastic volume strain corresponding to the residual internal friction angle
$\varepsilon_{v,\psi}^{p}$	plastic volume strain corresponding to the peak expansion angle
$\varepsilon^{exp}(t)$	test strain of the rheological test
$\varepsilon_t(X)$	strain at time t
$\Delta\sigma_m$	stress increment for the mth load
$J(t-t_m)$	creep compliance related to the parametric variable X
t_m	starting time of the mth load
t_T	total duration of the rheological test
N	times of multi-stage loading at t
$f_{ij}(X)$	objective function for identifying parameters
P_i	pore water pressure
P_c	confining pressure

Disclosure statement

The authors declare that they have no conflicts of interest.

Funding

The work was supported by the National Key Research and Development Project of China (Grant No. 2016YFC0401804), the Key projects of the Yalong River Joint Fund of the National Natural Science Foundation of China (Grant No. U1865203), and the National Science Foundation of China (Grant Nos. 51539002 and 51779018). It was also supported by the Basic Research Fund for Central Research Institutes of Public Causes (CKSF2017054/YT).

References

Barla, G., Debernardi, D., & Sterpi, D. (2012). Time-dependent modeling of tunnels in squeezing conditions. *International Journal of Geomechanics*, *12*(6), 697–710. doi:10.1061/(ASCE)GM.1943-5622.0000163

Boukharov, G. N., Chanda, M. W., & Boukharov, N. G. (1995). The three processes of brittle crystalline rock creep. *International Journal of Rock Mechanics and Mining Sciences & Geomechanics Abstracts*, *32*(4), 325–333. doi:10.1016/0148-9062(94)00048-8

Chan, K. S., Bodner, S. R., Fossum, A. F., & Munson, D. E. (1992). A constitutive model for inelastic flow and damage evolution in solids under triaxial compression. *Mechanics of Materials*, *14*(1), 1–14. doi:10.1016/0167-6636(92)90014-5

Chan, K. S., Bodner, S. R., Munson, D. E., & Fossum, A. F. (1996). Unelastic flow behavior of argillaceous salt. *International Journal of Damage Mechanics*, *5*(3), 292–314. doi:10.1177/105678959600500305

Chan, K. S., Brodsky, N. S., Fossum, A. F., Bodner, S. R., & Munson, D. E. (1994). Damage-induced nonassociated inelastic flow in rock salt. *International Journal of Plasticity*, *10*(6), 623–642. doi:10.1016/0749-6419(94)90026-4

Cristescu, N. D. (1987). Elastic/viscoplastic constitutive equations for rock. *International Journal of Rock Mechanics and Mining Sciences & Geomechanics Abstracts*, *24*(5), 271–282. doi:10.1016/0148-9062(87)90863-1

Cristescu, N. D. (1993). A general constitutive equation for transient and stationary creep of rock salt. *International Journal of Rock Mechanics and Mining Sciences & Geomechanics Abstracts*, *30*(2), 125–140. doi:10.1016/0148-9062(93)90705-I

Dashnor, H., Albert, G., & Francoise, H. (2005). Modelling long-term behavior of a natural gypsum rock. *Mechanics of Materials*, *37*(12), 1223–1241. doi:10.1016/j.mechmat.2005.06.002

Fabre, G., & Pellet, F. (2006). Creep and time-dependent damage in argillaceous rocks. *International Journal of Rock Mechanics and Mining Sciences*, *43*(6), 950–960. doi:10.1016/j.ijrmms.2006.02.004

Fahimifar, A., Karami, M., & Fahimifar, A. (2015). Modifications to an elasto-visco-plastic constitutive model for prediction of creep deformation of rock samples. *Soils and Foundations*, *55*(6), 1364–1371. doi:10.1016/j.sandf.2015.10.003

Feng, X. T., Zhang, C. Q., Qiu, S. L., Zhou, H., Jiang, Q., & Li, S. J. (2016). Dynamic design method for deep hard rock tunnels and its application. *Journal of Rock Mechanics and Geotechnical Engineering*, *8*(4), 443–461. doi:10.1016/j.jrmge.2016.01.004

Fossum, A. F., Brodsky, N. S., Chan, K. S., & Munson, D. E. (1993). Experimental evaluation of a constitutive model for inelastic flow and damage evolution in solids subjected to triaxial compression. *International Journal of Rock Mechanics and Mining Sciences & Geomechanics Abstracts*, *30*(7), 1341–1344. doi:10.1016/0148-9062(93)90119-X

Gioda, G. A. (1981). finite element solution of non-linear creep problems in rocks. *International Journal of Rock Mechanics and Mining Sciences & Geomechanics Abstracts*, *18*(1), 35–46. doi:10.1016/0148-9062(81)90264-3

Huang, S. L., Zhang, C. Q., & Ding, X., L. (2020). Hardening–softening constitutive model of hard brittle rocks considering dilatant effects and safety evaluation index. *Acta Mechanica Solida Sinica*, *33*(1), 121–140. doi:10.1007/s10338-019-00108-4

Liu, C., Zhou, F., Kang, J., & Xia, T. Q. (2016). Application of a non-linear viscoelastic-plastic rheological model of soft coal on borehole stability. *Journal of Natural Gas Science and Engineering*, *36*(B), 1303–1311. doi:10.1016/j.jngse.2016.03.026

Martin, C. D., & Chandler, N. A. (1994). The progressive fracture of Lac du Bonnet granite. *International Journal of Rock Mechanics and Mining Sciences & Geomechanics Abstracts*, *31*, 643–659. doi:10.1016/0148-9062(94)90005-1

Nedjar, B., & Roy, R. L. (2013). An approach to the modeling of viscoelastic damage application to the long-term creep of gypsum rock materials. *International Journal for Numerical and Analytical Methods in Geomechanics*, *37*(9), 1066–1078. doi:10.1002/nag.1138

Read, R. S., Chandler, N. A., & Dzik, E. J. (1998). The in situ strength criteria for tunnel design in highly stressed rock masses. *International Journal of Rock Mechanics and Mining Sciences & Sciences*, *35*, 319–368. doi:10.1016/S0148-9062(97)00302-1

Shen, Z. J. (2003). Breakage mechanics for geological materials: an ideal brittle-elasto-plastic model. *Chinese Journal Geotechnical Engineering*, *25*(3), 253–257.

Sterpi, D., & Gioda, G. (2009). Visco-plastic behaviour around advancing tunnels in squeezing rock. *Rock Mechanics and Rock Engineering*, *42*(2), 319–339. doi:10.1007/s00603-007-0137-8

Szczepanik, Z., Milne, D., Kostakis, K., & Eberhardt, E. (2003). Long term laboratory strength tests in hard rock. In 10th ISRM Congress, Sandton, South Africa, pp. 1179–1184.

Tang, H., Wang, D., Huang, R. Q., Pei, X. J., & Chen, W. L. (2018). A new rock creep model based on variable-order fractional derivatives and continuum damage mechanics. *Bulletin of Engineering Geology and the Environment*, *77*(1), 375–383. doi:10.1007/s10064-016-0992-1

Vyalov, S. S. (1986). *Rheologiacal fundamentals of soil mechanics* (O. K. Sapunov, Trans.) (pp. 147–190). Elsevier Science Publishing Company, Inc..

Wang, J-Y., Zhang, Y., Jia, Y., Jin, P.-J., & Zhu, L.-H. (2017). Elastoplastic modeling of mechanical behavior of weak rock at different time scales. *Journal of Central South University*, *24*(3), 699–707. doi:10.1007/s11771-017-3471-3

Wang, R., Zhuo, Z., Zhou, H. W., & Liu, J. F. (2017). A fractal derivative constitutive model for three stages in granite creep. *Results in Physics*, *7*, 2632–2638. doi:10.1016/j.rinp.2017.07.051

Zhang, J., Li, B., Zhang, C., & Li, P. (2019). Nonlinear viscoelastic–plastic creep model based on coal multistage creep tests and experimental validation. *Energies*, *12*(18), 3468–3473. doi:10.3390/en12183468

Zhang, Y., Shao, J. F., Xu, W. Y., & Jia, Y. (2016). Time-dependent behavior of cataclastic rocks in a multi-loading triaxial creep test. *Rock Mechanics and Rock Engineering*, *49*(9), 3793–3803. doi:10.1007/s00603-016-0948-6

Zhang, Y., Zhang, X. D., Shao, J. F., Jia, Y., & Wang, Y. L. (2018). Elastoplastic modelling the creep behaviour of cataclastic rock under multi-stage deviatoric stress. *European Journal of Environmental and Civil Engineering*, *22*(6), 650–665. doi:10.1080/19648189.2016.1217790

Zhang, C. Q., Zhou, H., & Feng, X. T. (2011). An Index for estimating the stability of brittle surrounding rock mass — FAI and its engineering application. *Rock Mechanics and Rock Engineering*, *44*(4), 401–414. doi:10.1007/s00603-011-0150-9

Zhao, B., Liu, D., Li, Z., Huang, W., & Dong, Q. (2018). Mechanical behavior of shale rock under uniaxial cyclic loading and unloading condition. *Advances in Civil Engineering*, *2018*, 1–8. doi:10.1155/2018/9750480